Modeling, Design, Control, and Implementation of a Modified Z-Source Integrated PV/Grid/EV DC Charger/Inverter

Siddhartha A. Singh, *Student Member, IEEE*, Giampaolo Carli, Najath A. Azeez, *Member, IEEE*, and Sheldon S. Williamson, *Senior Member, IEEE*

***Abstract*—Solar energy has been the most popular source of renewable energy for residential and semicommercial applications. Fluctuations of solar energy harvested due to atmospheric conditions can be mitigated through energy storage systems (ESS). Solar energy can also be used to charge electric vehicle batteries to reduce the dependence on the grid. One of the requirements for a converter for such applications is to have a reduced number of conversion stages and provide isolation. The Z-source inverter (ZSI) topology is able to remove multiple stages and achieve voltage boost and dc–ac power conversion in a single stage. The use of passive components also presents an opportunity to integrate ESS into them. This paper presents modeling, design, and operation of a modified ZSI integrated with a split primary isolated battery charger for dc charging of electric vehicle batteries. Simulation and experimental results have been presented for the proof of concept of the operation of the proposed converter.**

***Index Terms*—Active filter, distributed power generation, energy storage, inverter, photovoltaic (PV) power generation, quasi-Z-source inverter (qZSI), single-phase systems, solar energy, transportation electrification, Z-source inverters (ZSIs).**

I. Introduction

CHARGING of electric vehicles (EVs) at present heavily involves the use of an ac grid. Various methods of charging exclusively using an ac grid, such as wireless charging or plug-in charging, can still cause pollution irrespective of how highly efficient the topology is. The amount of fossil fuels that is consumed to generate the energy to charge an EV gives a clearer picture of the carbon footprint that is left behind while charging an EV. To achieve lower carbon footprints, one of the ways is to integrate renewable energy sources into a charging infrastructure to reduce the dependence on the ac grid.

A major requirement for designing an EV battery charger is the use of isolation transformers in the converter topologies to provide galvanic isolation at the user end from the rest of the high-voltage system as a safety measure [1].

The galvanic isolation can be provided either on the ac grid side or on the charger side. The size of the isolation transformer on the grid side is usually much larger than the one on the charger side [2]. Due to the improvement in semiconductor technology, high-frequency switching facilitates the use of smaller size transformers for galvanic isolation.

Photovoltaic (PV) grid interconnected systems have been used in the past for a commercial charging infrastructure [3]. These systems reduce the dependence of the charging infrastructure on the ac grid. The use of solar and grid interconnected systems is an attractive solution for residential charging systems for EVs. For systems up to 10 kW, single-phase inverters can be used for residential applications [4], [5]. For interconnection of the residential solar PV to the grid, various isolated and nonisolated topologies are available with multiple stages [4]–[9]. Residential PV systems for EV charging require features such as isolation and voltage boost capability to match the solar PV array voltage to the grid voltage requirements.

The Z-source inverter (ZSI) topology was first introduced in [10]. It has an ability to buck or boost and invert the input dc voltage in a single stage. It has gained tremendous interest in PV-grid-connected applications. The ZSI topology uses two capacitors and two inductors to boost the input dc voltage to match the inverter-side ac output voltage requirements. The operation of a ZSI is heavily dependent on the passive components. It presents an opportunity to integrate energy storage units into such a system.

In this paper, a proof of concept of a single-phase modified Z-source inverter (MZSI)-based solar grid-connected charger has been presented as an application toward a string inverter configuration. In Section II, the basic operation principle for a ZSI has been discussed along with the component design. Section III discusses the component sizing, modeling, and control of the converter. Section IV presents the simulation results for the operation of a 3.3-kW proposed inverter charger and the results from an experimental setup built as a proof of concept. Section V presents the conclusion.

Manuscript received July 31, 2017; revised October 24, 2017; accepted November 22, 2017. Date of publication December 18, 2017; date of current version February 13, 2018. *(Corresponding author: Siddhartha A. Singh.)*

S. A. Singh, N. A. Azeez, and S. S. Williamson are with the Smart Transportation Electrification and Energy Research Group, Department of Electrical, Computer, and Software Engineering, University of Ontario Institute of Technology, Oshawa, ON L1H 7K4, Canada (e-mail: siddhartha.anirban87@gmail.com; najath@gmail.com; sheldon.williamson@uoit.ca).

G. Carli is with EMD Technologies, Saint-Eustache, QC J7R 0A1, Canada (e-mail: giampaolocarli@gmail.com).

Color versions of one or more of the figures in this paper are available online at http://ieeexplore.ieee.org.

Digital Object Identifier 10.1109/TIE.2017.2784396

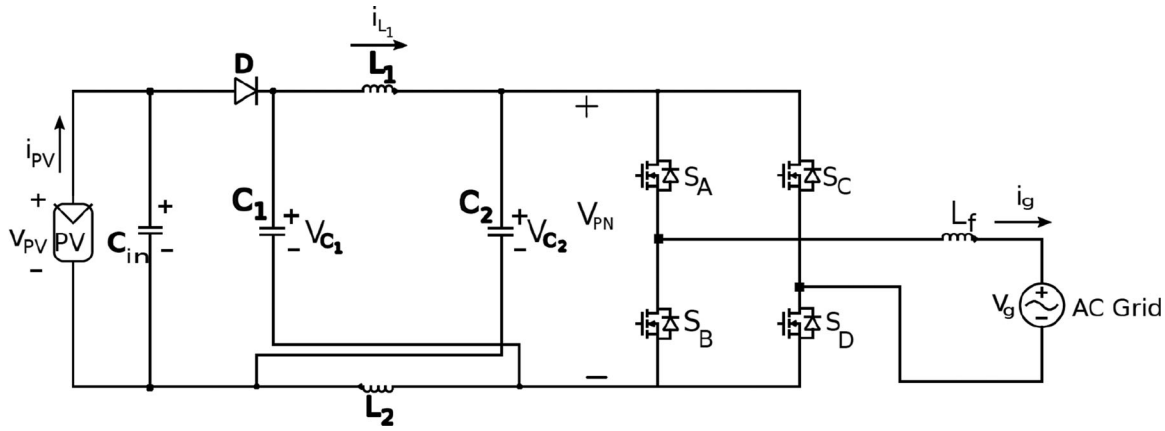

Fig. 1. Schematic of a PV/ac grid interconnected ZSI.

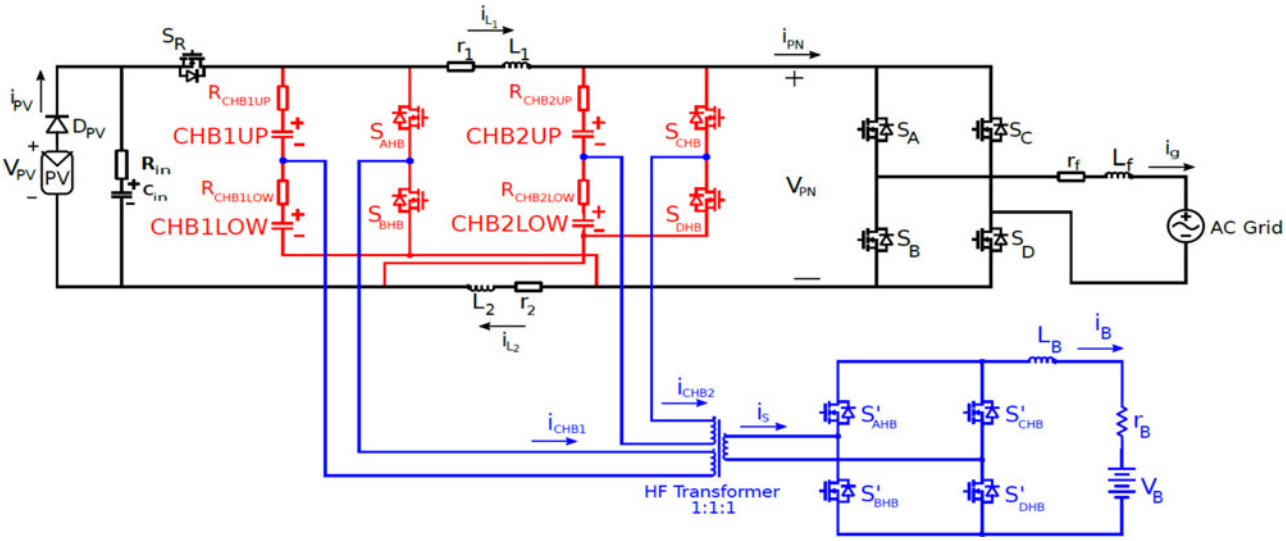

Fig. 2. Detailed schematic of the proposed MZSI.

II. Traditional ZSI

The ZSI topology, shown in Fig. 1, utilizes two modes of operation: the shoot-through state and the nonshoot-through state [10]. For symmetrical operations, we have

$$i_L = i_{L1} = i_{L2} \tag{1}$$

$$V_C = V_{C1} = V_{C2}. \tag{2}$$

From Fig. 1, in the shoot-through state, all four switches S_1, S_3, S_2 and S_4, are conducting at the same time. The duration of this shoot-through state is described by the duty cycle D_0 and the switching frequency F_{SW}.

The shoot-through state can be implemented by a modified pulse width modulation (PWM) technique presented in [10].

Therefore, the two capacitor voltages are expressed as [10]

$$V_C = \frac{1 - D_0}{1 - 2D_0} v_{pv}. \tag{3}$$

The peak dc-link voltage $\hat{V_{PN}}$ is given by [10]

$$\hat{V_{PN}} = \frac{1}{1 - 2D_0} v_{pv}. \tag{4}$$

The power balance equation between the dc and ac sides of the ZSI is expressed as [10]

$$(1 - D_0)\hat{V_{PN}} I_{PN} = i_{grms} v_{grms} \tag{5}$$

where I_{PN} and $\hat{V_{PN}}$ are the peak dc-link current and voltage, respectively. The peak ac voltage of the ZSI is [10]

$$V_g = M\hat{V_{PN}} \tag{6}$$

where M is the modulation index, the grid voltage $v_g = V_g \sin \omega t$, and the grid current $i_g = I_g \sin(\omega t + \phi)$ for $\phi = 0$ for grid-connected applications. From (11) and (13), the RMS of the output ac voltage of the ZSI is [10]

$$V_{grms} = \frac{M v_{pv}}{\sqrt{2}(1 - 2D_0)}. \tag{7}$$

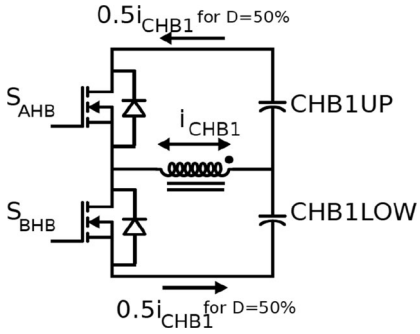

Fig. 3. Schematic of one the primary across CHB1 operating at 50% duty cycle.

III. Component Sizing, Modeling, and Control of the Proposed MZSI

Fig. 2 shows that an MZSI has been proposed having an integrated charger. The two capacitors C_1 and C_2 from Fig. 1 are split, and each of them acts as one of the legs of one of the two primaries of the split primary isolated half-bridge converter (HBC). The MOSFET S_R allows bidirectional operation of the MZSI when required. The diode $D_{\rm PV}$ blocks the reverse flow of the current back into the PV. $R_{\rm in}$ is the internal resistance of the input capacitor $C_{\rm in}$. For a symmetrical operation of the MZSI, a split primary isolated dc-to-dc converter has been proposed for the integration of the charger side into the ZSI. The split primaries contain two HBC primaries isolated from a single full-bridge secondary through a high-frequency transformer. The HBC primaries and the secondaries are operated at 50% duty cycle in an open loop. The output current of the secondary is connected to an energy storage unit such as a lithium-ion battery. The energy storage unit clamps its own voltage v_B across the input of the HBC primaries, V_C, such that

$$V_C = 2v_B. \tag{8}$$

A. Maximum Shoot-Through Duty Ratio, D_{0max}

As a result of the energy storage unit being connected across the capacitors, the maximum shoot-through duty ratio $D_{0\rm max}$ is calculated based on the minimum input voltage $v_{\rm pvmin}$ and the maximum battery voltage $V_{B\rm max}$ connected across the capacitors and is expressed as

$$D_{0\rm max} = \frac{2V_{B\rm max} - v_{\rm pvmin}}{4V_{B\rm max} - v_{\rm pvmin}}. \tag{9}$$

SAE J1772 standard defines the standard battery voltages for dc charging between 200 and 500 V.

B. Inductor L_1 and L_2 Design

The inductors L_1 and L_2 are sized for high-frequency peak-to-peak current ripple assumed between 15% and 25% of the inductor current during the shoot-through time interval $\frac{D_0 T}{2}$ as follows [11]:

$$L_1 = L_2 = \frac{V_{C\rm max} D_{0\rm max}}{2\Delta i_L f}. \tag{10}$$

C. Capacitor C_1 and C_2 Design

The capacitors are sized to absorb the second-order harmonic component in the capacitor voltages as follows [11]:

$$C_1 = C_2 = \frac{P}{2\omega \Delta V_C V_C} \tag{11}$$

where V_C is the average voltage across the capacitors V_{C1} and V_{C2}, and ΔV_C is the predetermined voltage ripple limit. ω is the second-order harmonics expressed in rad/s.

In single-phase ZSIs, oversized electrolytic capacitors for second-order harmonic suppression can result in a bulky system. A dc-side active power filter proposed in [12] can be used to reduce the required capacitance. It operates independently of the operation of the MZSI.

For the proposed topology, the maximum capacitor voltage rating is equal to at least twice the peak voltage of the energy storage device clamped across it.

D. Average Modeling of the Integrated Half-Bridge DC–DC Converter Charger

When an energy storage unit is connected to the secondary side of the charger, then each of the split primaries operates alternately and supplies half of the required battery current. Each of the primaries of the dc–dc converter is connected across the capacitors of either legs. The voltage across the capacitors is defined by (15). The detailed average modeling of the split primary dc–dc converter is explained in [13]. Each of the two primaries can be represented using an RLE circuit connected parallel to each of the capacitors C_1 and C_2, as shown in the simplfied equivalent model of Fig. 4.

E. State-Space Average Modeling of the Single-Stage Inverter Charger

The detailed state-space average modeling was presented in [10]. The equivalent diagram of the modeled MZSI is shown in Fig. 4. During the nonshoot-through state, the Kirchhoff's voltage law (KVL) equation is given by

$$L\frac{di_L}{dt} = v_{\rm pv} - i_L r + R_{\rm HB} + \left(2\hat{i_g} + \frac{i_B}{2}\right) R_{\rm HB} - V_C. \tag{12}$$

The Kirchhoff's current law (KCL) equation is

$$C\frac{dV_C}{dt} = i_L - \hat{i_g} - \frac{i_B}{4}. \tag{13}$$

During the shoot-through state, the KVL equation is

$$L\frac{di_L}{dt} = V_C - i_L(R_{\rm HB} + r) - \frac{i_B}{2} R_{\rm HB}. \tag{14}$$

The KCL equation is written as

$$C\frac{dV_C}{dt} = -i_L - \frac{i_B}{4}. \tag{15}$$

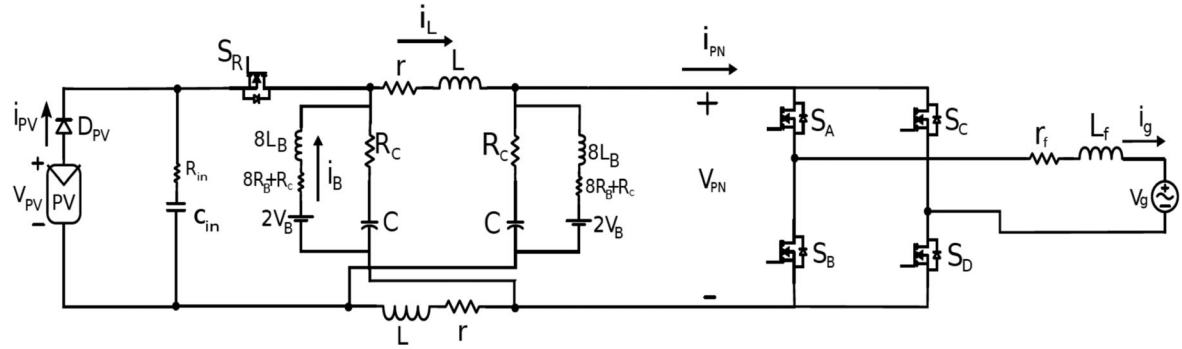

Fig. 4. Equivalent model of the proposed MZSI with a battery.

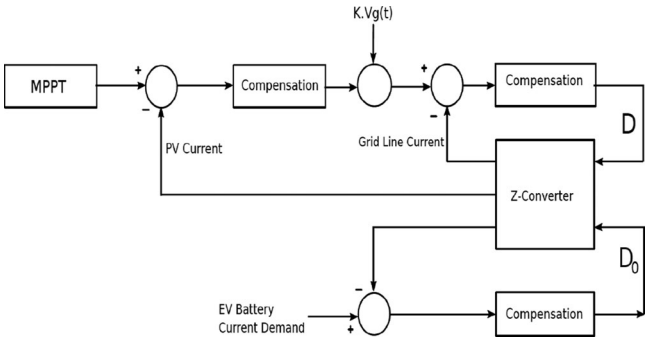

Fig. 5. Block diagram of the control scheme of the proposed MZSI charger.

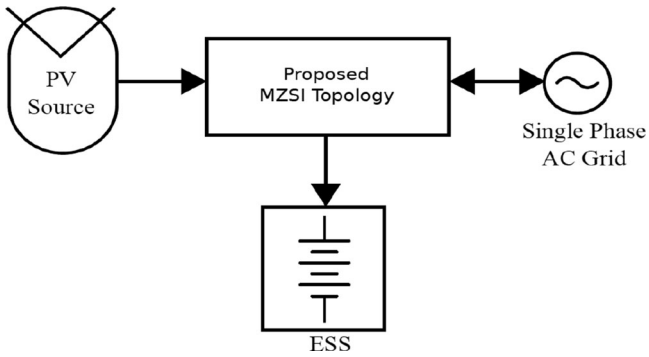

Fig. 6. Simplified block diagram of the system.

From (12)–(15), state-space equations for the entire system can be written as

$$\begin{bmatrix} \dot{i}_L \\ \dot{V}_C \\ \dot{i}_B \end{bmatrix} = \begin{bmatrix} -\frac{-(r+2R_{\rm HB})}{L} & -\frac{1-2D_0}{L} & \frac{(1-2D_0)}{2}R_{\rm HB} \\ \frac{1-2D_0}{C} & 0 & -\frac{1}{4C} \\ \frac{1-2D_0}{L_B}R_{\rm HB} & \frac{1}{2L_B} & -\frac{R_{\rm HB}+R_B}{2L_B} \end{bmatrix} \begin{bmatrix} i_L \\ V_C \\ i_B \end{bmatrix} + \begin{bmatrix} \frac{2(1-D_0)R_{\rm HB}}{L} \\ -\frac{1-D_0}{C} \\ -\frac{(1-D_0)R_{\rm HB}}{L_B} \end{bmatrix} \begin{bmatrix} i_d \end{bmatrix} + \begin{bmatrix} \frac{(1-D_0)}{L} \\ 0 \\ 0 \end{bmatrix} \begin{bmatrix} v_{\rm pv} \end{bmatrix} + \begin{bmatrix} 0 \\ 0 \\ -\frac{1}{L_B} \end{bmatrix} \begin{bmatrix} V_B \end{bmatrix}. \quad (16)$$

Fig. 4 shows the positive directions of the battery current i_B and the grid-side ac current i_g.

Fig. 5 shows the block diagram for the controller for the proposed MZSI topology. It consists of three loops: the PV current $i_{\rm pv}$ loop, the grid current i_g loop, and the battery current i_B loop.

In the literature, the ZSI capacitor voltage is controlled to generate the reference current for the H-bridge inverter output current [14] or generate the shoot-through duty ratio D_0 [15]. In this paper, the reference current is generated by controlling the peak input PV current [16]. If a stiff voltage V_C is connected across either or both capacitors, the shoot-through duty ratio D_0 will depend on V_C.

Since the battery current loop does not require fast dynamic changes, battery loop control is the slowest response compared to the input current control. For the battery loop control, the transfer function is given by

$$\frac{I_B(s)}{d_0(s)} = \frac{-sC[4R_{\rm HB}i_L - 2R_{\rm HB}i_d] - [2i_L - i_d]}{2L_BCs^2 + sC[R_{\rm HB} + 2R_B] + 0.25}. \quad (17)$$

A feedforward is added to the battery control loop:

$$\mathrm{FF}_B = \frac{2V_B - v_{\rm PV}}{4V_B - v_{\rm PV}} \quad (18)$$

where V_B is the output voltage of the HBC and $v_{\rm PV}$ is the tracked PV voltage.

The output ac-side current controller should have the fastest response.

F. Energy Management Scheme for the Proposed Converter

Fig. 6 shows a simplified block diagram of the proposed system. When an energy storage system (ESS) is integrated into a ZSI, (5) is modified as follows [14]:

$$v_{\rm PV}i_{\rm PV} = v_b i_b + i_{g\rm rms}v_{g\rm rms} \quad (19)$$

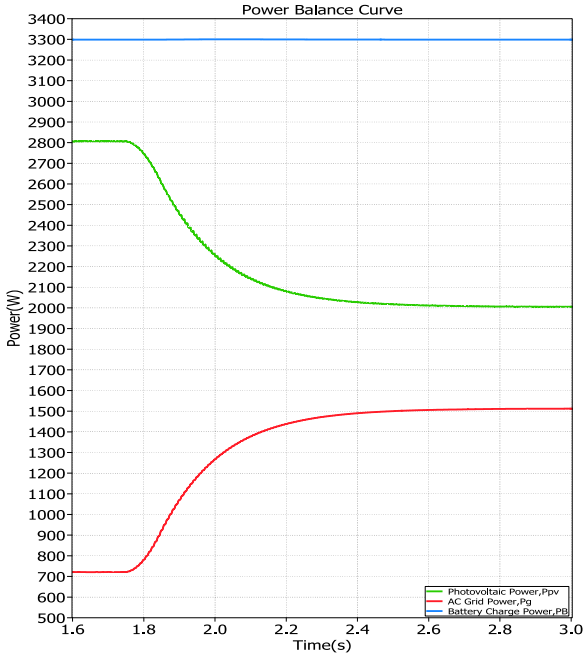

Fig. 7. Simulation waveform for the power balance between the PV input power, the ac grid side, and the battery power.

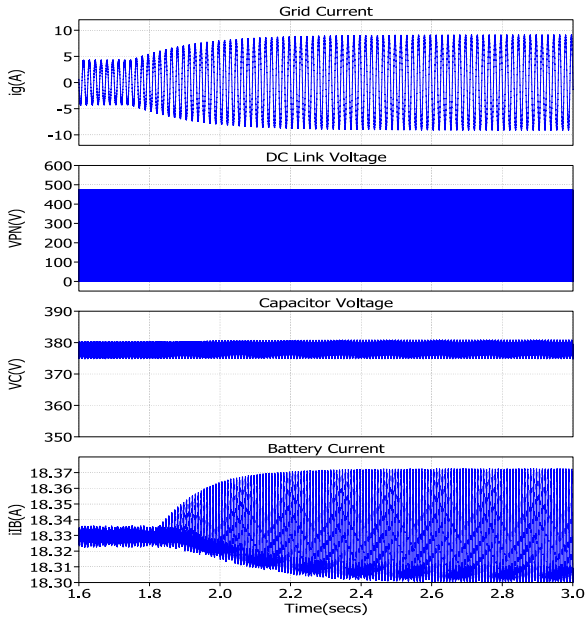

Fig. 8. Simulation waveform of the grid current I_g, the dc-link voltage V_{PN}, the capacitor voltage V_{C1}, and the battery current i_b for the power balance between the PV input power, the ac grid side, and the battery power.

where i_b and v_b are the battery current and voltage, respectively.

Fig. 6 shows that the single-phase ac grid power P_g balances the power fluctuation of the PV source P_{pv}; thus, a constant charge power P_B is obtained at the ESS.

For EV battery charging using both the single-phase ac grid and the PV power, the direction of the ac grid current i_g changes to negative while drawing power from the grid.

The inverter side can be operated bidirectionally, and the PV and the grid provide power for the charger, maintaining the power balance

$$v_{\text{PV}} i_{\text{PV}} + i_{g\text{rms}} v_{g\text{rms}} = v_b i_b. \tag{20}$$

As long as the voltage across the input capacitor C_{in} is maintained to at least the minimum value of the PV voltage, the MZSI can be operated as a grid-connected rectifier/charger in the absence of the PV [18]–[21].

Antiislanding protection techniques for the ZSI topology have been addressed in the literature previously in [22].

IV. Simulation and Experimental Results

A. Simulation Study for an MZSI Operation

The simulation studies to demonstrate the behavior of the proposed topology have been carried out using PLECS 4 for a 3.3-kW charger for a string inverter configuration. Simulation has been carried out for the system shown in Fig. 2.

Fig. 7 shows that at a simulation time $t = 1.75$ s, the input PV power reduces from 2.8 to 2 kW and the grid power increases from 710 to 1500 W to maintain the output charger power to 3.3 kW. The corresponding grid current, the dc-link voltage, the capacitor voltage, and the battery current are shown in Fig. 8.

TABLE I
MZSI-Based Charger System Simulation Specifications

Parameters	Value
Input voltage, V_{in}	286 V
Input current, I_{in}	9.8 A
Inductor value, $L_1 = L_2$	500 μH
ZSI switching frequency, F_{SW}	25 kHz
Grid voltage (RMS), V_g	240 V
Inverter output filter inductor, L_f	7.5 mH
PV input power, P_{PV}	2.8 kW
Input capacitor, C_{in}	2 mF
HBC switching frequency, f	50 kHz
HBC output filter, L_B	1 mH
Battery charge power, P_B	3.3 kW

TABLE II
Component Models Used for Loss Modeling of the Proposed System

Component	Value
Diode, D	STTH6010W
ZSI MOSFETs [S_A, S_B, S_C, and S_D]	APT28M120L
HBC MOSFETs [S_{AHB}, S_{BHB}, S_{CHB} and S_{DHB}]	APT28M120L
HBC diodes [S'_{AHB}, S'_{BHB}, S'_{CHB} and S'_{DHB}]	STTH6010W
Capacitors C_{in}, C_1, and C_2	ECE-T2VP182FA

B. Loss Modeling

The loss modeling for the proposed system shown in Fig. 2 has been carried out by modeling the actual components in PLECS 4.0. The switching components used for the modeling are shown in Table II.

For the loss modeling of the passive components, the internal resistance of the inductors L_1, L_2, and L_f is given as $r =$

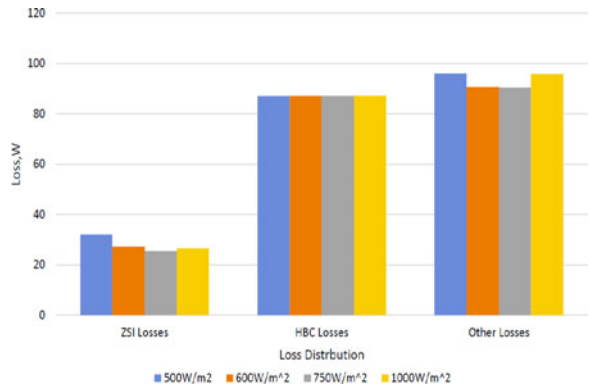

Fig. 9. Loss distribution chart for the MZSI topology for a fixed charging power $P_B = 3.3$ kW at 25 °C under varying irradiation.

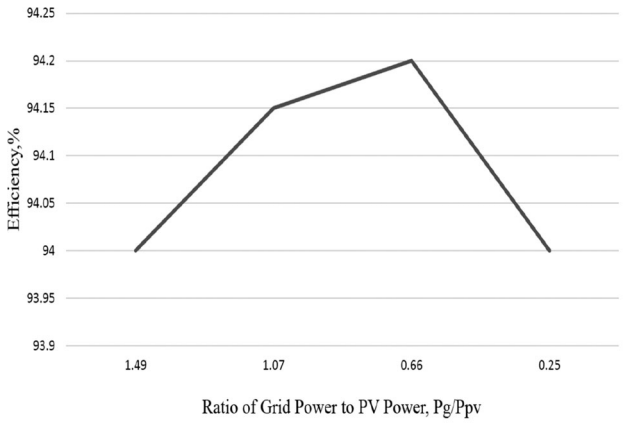

Fig. 10. Efficiency curve for different ratios of ac grid power P_g to PV power P_{pv} curve for a fixed charging power $P_B = 3.3$ kW at 25 °C under varying irradiation.

100 mΩ, and the equivalent series resistance R_{HB} for the capacitors $C1$, C_2, and C_{in} is 138 mΩ.

Fig. 9 shows the loss distribution between the ZSI (conduction and switching losses of the MOSFETs and diode D), the HBC (conduction and switching losses of the MOSFETs and secondary diodes), and other losses is due to the inductor, capacitors, leakage losses in the high-frequency transformer, and battery series resistances in the system for varying irradiations for a constant charging power $P_B = 3.3$ kW.

Fig. 10 shows that the efficiency is around 94% from the efficiency curve for various ratios of the ac grid power P_g to the PV power P_{pv} for a fixed charging power $P_B = 3.3$ kW at 25 °C, for varying irradiation between 500 and 1000 W/m^2. Although the efficiency variations are small, the efficiency is the highest when the sharing between the PV power P_{pv} and the grid power P_g is equal.

For a constant frequency of operation, the HBC MOSFET losses remain constant for a fixed value V_B and charging power P_B, although, in reality, this might not be the case. The efficiency of the converter will change with the change in the battery voltage. Fig. 11 shows the distribution of the losses between the ZSI losses, the HBC MOSFETs, and the losses due to the

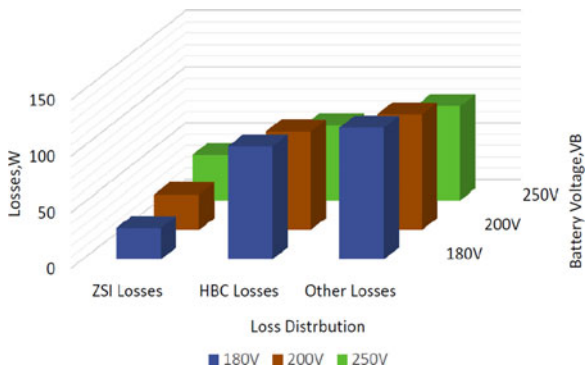

Fig. 11. Loss distribution for various battery voltages V_B for a fixed charging power $P_B = 3.3$ kW at 45 °C.

TABLE III
MZSI-BASED CHARGER SYSTEM PROTOTYPE ELECTRICAL SPECIFICATIONS

Parameters	Value
Input voltage, V_{in}	38 V
Input current, I_{in}	3.82 A
Inductor values, L_1 and L_2	500 μH
Peak dc-link voltage, V_{PN}	63.33 V
Modulation index, M	0.75
Shoot-through duty ratio, D_{0max}	0.2
Switching frequency, F_{SW}	25 kHz
Grid voltage, V_g	34 V(RMS)
Inverter output filter inductor, L_f	2.5 mH
HBC switching frequency, f_{HBC}	50 kHz

TABLE IV
ISOLATED HALF-BRIDGE DC–DC SYSTEM ELECTRICAL SPECIFICATIONS

Parameters	Value
Input voltage, V_C	50.667 V
Output voltage, V_B	25.335 V
Switching frequency, $F_{sw(HB)}$	50 kHz
Filter inductor, L_B	330 μH

inductor, capacitors, leakage losses in the high-frequency transformer, and battery series resistances in the system for various battery voltages. As shown in Fig. 11, at 45 °C , the v_{pv} drops to 258 V, and it can be observed that with the increase in the battery voltage, the ZSI losses increase, but the HBC losses and the losses in the passive components reduce.

C. Experimental Verification of the MZSI Power Balance Operation

In this paper, as a proof of concept, a scaled-down 175-W experimental setup was built using MATLAB/Simulink and dSPACE 1103. The setup has the specifications shown in Table III.

Fig. 12 shows the PWM scheme for the HBC. Each of the split primary operates for half of the HBC switching period. Each of the MOSFETs S_{AHB}, S_{BHB}, S_{CHB}, and S_{DHB} operates exclusively for one-quarter of the entire HBC switching period. Equation (23) can be written in terms of the current sharing

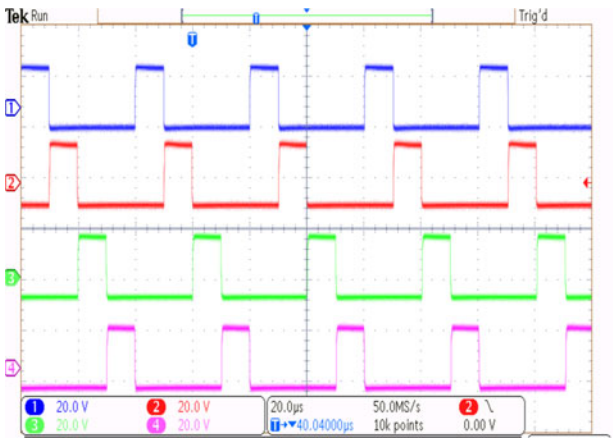

Fig. 12. PWM logic for the isolated HBC.

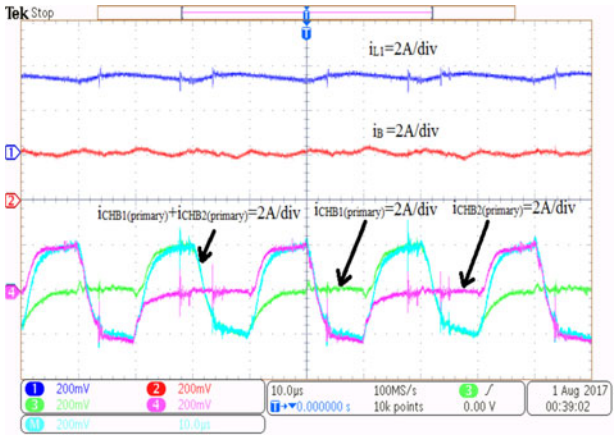

Fig. 13. Experimental setup waveforms for the inductor current (top), charger output current (middle), and the primary currents of the split charger (bottom).

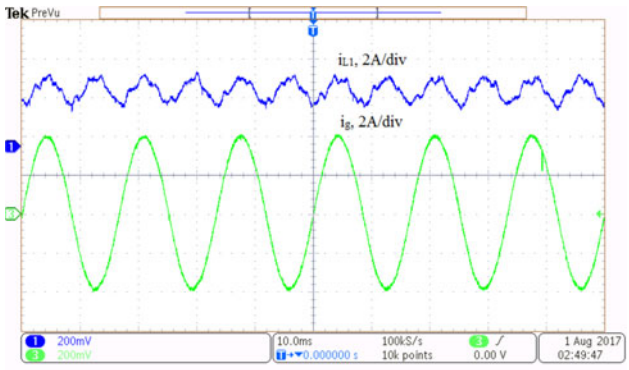

Fig. 14. Experimental waveform input current (blue) and output current (green) between the charger and the ac output of the MZSI.

between the ac load (grid) and the battery as

$$i_{\mathrm{PV}} = \frac{1 - D_0}{2(1 - 2D_0)} i_b + \frac{M}{\sqrt{2}(1 - 2D_0)} i_g. \tag{21}$$

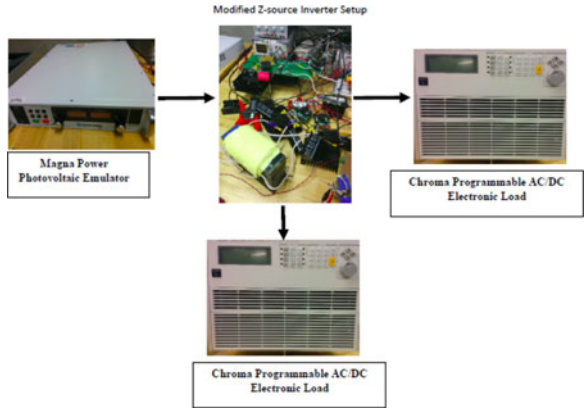

Fig. 15. Experimental setup.

where M is the modulation index and D_0 is the shoot-through duty ratio. For $D_0 = 0.2$, we have

$$i_{\mathrm{PV}} = \frac{2}{3} i_b + \frac{\sqrt{3}}{2} i_g. \tag{22}$$

From (22), at $D_0 = 0.2$, for an input current $i_{\mathrm{PV}} = 3.82$ A and a fixed HBC output current $i_b = 2$ A, the ZSI ac output current i_g is calculated to be 2.87 A.

Fig. 13 shows the inductor current i_{L1}, the battery current i_B, the split primary current i_{CHB1} and i_{CHB2}, and the total primary current. Each of the primary operates alternately. The total primary current is a high-frequency alternating current of $f_{\mathrm{HBC}} =$ 50 kHz.

As shown in Figs. 13 and 14, the charger output current is maintained at 2 A using a Chroma Programmable AC/DC Electronics Load (Model 6304). The PV input current is maintained at 3.82 A using a Magna-power LXI solar emulator. The output grid current is observed to be 2.66 A. Fig. 15 shows the experimental setup for the proof of concept.

The lower values of the output current are a result of the losses in the circuit. The practical PI value for the ac-side current control was $K_P = 0.03$, the battery loop was $K_{PB} = 0.0003$ and $K_{IB} = 0.09$, and the input PV current loops were $K_{P\mathrm{in}} = 0.005$ and $K_{I\mathrm{in}} = 2$.

V. Conclusion

A MZSI topology proposed in this paper is an attractive solution for PV-grid-connected charging systems. It consists of a single-stage PV-grid connection and an integrated charger for PV-grid-connected charging or energy storage. This topology can be applied to a centralized configuration for charging in semicommercial locations such as a parking lot of a shopping mall. For residential applications, this idea can be extended to string inverters with the charger side of the string inverter configurations connected in series or parallel for current sharing. This paper proposed an energy storage topology using a Z-source converter through a symmetrical operation of its impedance network.

REFERENCES

[1] D. Aggeler *et al.*, "Ultra-fast dc-charge infrastructures for EV-mobility and future smart grids," in *Proc. IEEE PES Innovative Smart Grid Technol. Conf. Eur.*, Oct. 2010, pp. 1–8.

[2] G. Carli and S. S. Williamson, "Technical considerations on power conversion for electric and plug-in hybrid electric vehicle battery charging in photovoltaic installations," *IEEE Trans. Ind. Electron.*, vol. 28, no. 12, pp. 5784–5792, Dec. 2013.

[3] J. G. Ingersoll and C. A. Perkins, "The 2.1 kW photovoltaic electric vehicle charging station in the city of Santa Monica, California," in *Proc. 25th IEEE Photovoltaic Spec. Conf.*, May 1996, pp. 1509–1512.

[4] S. B. Kjaer, J. K. Pedersen, and F. Blaabjerg, "A review of single-phase grid-connected inverters for photovoltaic modules," *IEEE Trans. Ind. Appl.*, vol. 41, no. 5, pp. 1292–1306, Sep. 2005.

[5] N. A. Ninad, L. A. C. Lopes, and I. S. Member, "Operation of single-phase grid-connected inverters with large DC bus voltage ripple," *Proc. IEEE Can. Elect. Power Conf.*, 2007, pp. 172–176.

[6] S. V. Araujo, P. Zacharias, and R. Mallwitz, "Highly efficient single-phase transformerless inverters for gridconnected photovoltaic systems," *IEEE Trans. Ind. Electron.*, vol. 57, no. 9, pp. 3118–3128, Sep. 2010.

[7] D. Meneses, F. Blaabjerg, O. García, and J. A. Cobos, "Review and comparison of step-up transformerless topologies for photovoltaic ac-module application," *IEEE Trans. Power Electron.*, vol. 28, no. 6, pp. 2649–2663, Jun. 2013.

[8] R. Gonzalez, J. Lopez, P. Sanchis, and L. Marroyo, "Transformerless inverter for single-phase photovoltaic systems," *IEEE Trans. on Power Electron.*, vol. 22, no. 2, pp. 693–697, Mar. 2007.

[9] S. Bai, D. Yu, and S. Lukic, "Optimum design of an EV/PHEV charging station with dc bus and storage system," in *Proc. IEEE Energy Convers. Congr. Expo.*, Sep. 2010, pp. 1178–1184.

[10] F. Z. Peng, "Z-source inverter," *IEEE Trans. Ind. Appl.*, vol. 39, no. 2, pp. 504–510, Mar./Apr. 2003.

[11] Y. Huang, M. Shen, F. Z. Peng, and J. Wang, "Z-source inverter for residential photovoltaic systems," *IEEE Trans. Power Electron.*, vol. 21, no. 6, pp. 1776–1782, Nov. 2006.

[12] S. A. Singh, N. A. Azeez, and S. S. Williamson, "Capacitance reduction in a single phase quasi z-source inverter using a hysteresis current controlled active power filter," in *Proc. IEEE 25th Int. Symp. Ind. Electron.*, Jun. 2016, pp. 805–810.

[13] S. A. Singh, G. Carli, N. A. Azeez, and S. S. Williamson, "A modified z-source converter based single phase PV/grid inter-connected dc charging converter for future transportation electrification," in *Proc. IEEE Energy Convers. Congr. Expo.*, Sep. 2016, pp. 1–6.

[14] Y. Li, S. Jiang, J. G. Cintron-Rivera, and F. Z. Peng, "Modeling and control of quasi-z-source inverter for distributed generation applications," *IEEE Trans. on Ind. Electron.*, vol. 60, no. 4, pp. 1532–1541, Apr. 2013.

[15] T. Chandrashekhar and M. Veerachary, "Control of single-phase z-source inverter for a grid connected system," in *Proc. Int. Conf. Power Syst.*, Dec. 2009, pp. 1–6.

[16] B. Ge *et al.*, "Current ripple damping control to minimize impedance network for single-phase quasi-z source inverter system," *IEEE Trans. Ind. Informat.*, vol. 12, no. 3, pp. 1043–1054, Jun. 2016.

[17] B. Ge *et al.*, "An energy-stored quasi-z-source inverter for application to photovoltaic power system," *IEEE Trans. Ind. Electron.*, vol. 60, no. 10, pp. 4468–4481, Oct. 2013.

[18] J. Rabkowski, R. Barlik, and M. Nowak, "Pulse width modulation methods for bidirectional/high-performance z-source inverter," in *Proc. IEEE Power Electron. Spec. Conf.*, Jun. 2008, pp. 2750–2756.

[19] A. Battiston, E. H. Miliani, J. P. Martin, B. Nahid-Mobarakeh, S. Pierfederici, and F. Meibody-Tabar, "A control strategy for electric traction systems using a pmmotor fed by a bidirectional z-source inverter," *IEEE Trans. Vehicular Tech.*, vol. 63, no. 9, pp. 4178–4191, Nov. 2014.

[20] O. Ellabban, J. V. Mierlo, and P. Lataire, "Control of a bidirectional z-source inverter for hybrid electric vehicles in motoring, regenerative braking and grid interface operations," in *Proc. IEEE Elect. Power Energy Conf.*, Aug. 2010, pp. 1–6.

[21] S. Dong, Q. Zhang, and S. Cheng, "Analysis of critical inductance and capacitor voltage ripple for a bidirectional z -source inverter," *IEEE Trans. Power Electron.*, vol. 30, no. 7, pp. 4009–4015, Jul. 2015.

[22] M. Trabelsi and H. Abu-Rub, "A unique active anti-islanding protection for a quasi-z-source based power conditioning system," in *Proc. IEEE Appl. Power Electron. Conf. Expo.*, Mar. 2015, pp. 2237–2243.

Siddhartha A. Singh (S'10) received the B.Tech. degree from West Bengal University of Technology, Kolkata, India, in 2009 and the M.Tech. degree from Vellore Institute of Technology, Vellore, India, in 2011 (specializing in power electronics and motor drives), both in electrical engineering. He is currently working toward the Ph.D. degree in electrical engineering with the Smart Transportation Electrification and Energy Research Group, Department of Electrical, Computer, and Software Engineering, University of Ontario Institute of Technology, Oshawa, ON, Canada.

His current research interests include photovoltaic converters, electric vehicle battery chargers, and power electronics converter development.

Giampaolo Carli received the bachelor's degree in electrical engineering from McGill University, Montreal, QC, Canada, in 1984, and the M.S. degree in electrical engineering (with specialization in electric vehicle charging technology and infrastructure) from Concordia University, Montreal, in 2009.

He is a Power Electronics Specialist working on the domain of high-voltage generation for X-ray systems with EMD Technologies, Saint-Eustache, QC. He devoted many years to the power electronics industry in various fields ranging from industrial and commercial computer systems to telecom.

Najath A. Azeez (M'99) received the B.Tech. degree from the National Institute of Technology, Calicut, India, in 2003, and the M.Tech. and Ph.D. degrees from the Indian Institute of Science, Bangalore, India, in 2008 and 2014, respectively, all in electrical engineering, with focus on power electronics and motor drives.

He is currently a Postdoctoral Fellow with the University of Ontario Institute of Technology, Oshawa, ON, Canada. His research interests include power converters and drives.

Sheldon S. Williamson (S'01–M'06–SM'13) received the B.E. (Hons.) degree from the University of Mumbai, Mumbai, India, in 1999, and the M.S. and Ph.D. (Hons.) degrees from the Illinois Institute of Technology, Chicago, IL, USA, in 2002 and 2006, respectively, all in electrical engineering, with a focus on automotive power electronics and motor drives at the Grainger Power Electronics and Motor Drives Laboratory.

From 2006 to 2011, he was a Tenure-Track Assistant Professor with the Department of Electrical and Computer Engineering, Concordia University, Montreal, QC, Canada, where he was a Tenured Associate Professor from 2011 to 2014. He is currently an Associate Professor with the Smart Transportation Electrification and Energy Research Group, Department of Electrical, Computer, and Software Engineering, University of Ontario Institute of Technology, Oshawa, ON, Canada. His current research interests include advanced power electronics and motor drives for transportation electrification, electric energy storage systems, and electric propulsion.

Dr. Williamson was the Natural Sciences and Engineering Research Council of Canada's Research Chair of Electric Energy Storage Systems for Transportation Electrification.